Deep-UV 236.5 nm laser by fourth-harmonic generation of a single-crystal fiber Nd:YAG oscillator

Loïc Deyra, Igor Martial, Julien Didierjean, François Balembois, Patrick Georges

HAL Id: hal-01304704

https://hal-iogs.archives-ouvertes.fr/hal-01304704

Submitted on 20 Apr 2016

Deep-UV 236.5 nm laser by fourth-harmonic generation of a single-crystal fiber Nd:YAG oscillator

Loïc Deyra,[1,*] Igor Martial,[2] Julien Didierjean,[2] François Balembois,[1] and Patrick Georges[1]

[1]*Laboratoire Charles Fabry, Institut d'Optique, CNRS, Univ Paris-Sud, 91127 Palaiseau, France*

[2]*Fibercryst SAS, Parc d'activité Wilson, Bât A1, 31 Rue Wilson, 69150 Dcines Charpieu, France*

Corresponding author: loic.deyra@institutoptique.fr

We demonstrate a deep-UV laser at 236.5 nm based on extracavity fourth-harmonic generation of a Q-switched Nd:YAG single-crystal fiber laser at 946 nm. We first compare two nonlinear crystals available for second-harmonic generation: LBO and BiBO. The best results at 473 nm are obtained with a BiBO crystal, with an average output power of 3.4 W at 20 kHz, corresponding to a second-harmonic generation efficiency of 38%. This blue laser is frequency-converted to 236.5 nm in a BBO crystal with an overall fourth-harmonic generation yield of 6.5%, corresponding to an average output power of 600 mW at 20 kHz. This represents an order of magnitude increase in average power and energy compared to previously reported pulsed lasers at 236.5 nm. This work opens the possibility of LIDAR detection of dangerous compounds for military or civilian applications.

The development of deep-UV solid-state lasers based on nonlinear frequency conversion has opened applications previously based on excimer lasers, such as material processing or spectroscopy applications. The most common approach is fourth-harmonic generation of the 1064 nm laser line of Nd:YAG, which has been a commercial product for many years. Unfortunately, important applications, such as manufacturing of Bragg gratings or waveguides, would be more efficient using wavelengths below 250 nm. Moreover, some particular spectroscopic applications, such as detection of dangerous compounds, require specific wavelengths in the deep-UV. One possible solution is to use a fundamental laser operating at a lower wavelength, such as the 946 nm laser line of Nd:YAG. Subsequent fourth-harmonic generation leads to a wavelength of 236.5 nm, which lies in the absorption band of molecules related to improvised explosive devices or nuclear, radiological, biological, and chemical components [1,2]. The challenge is to obtain enough pulse energy to increase the detection range and accuracy. Unfortunately, previous works at 236.5 nm only demonstrated a maximum energy of 500 nJ [3,4], with an average power of 20 mW. This energy limitation comes from the difficulty to obtain significant laser output in Nd:YAG at 946 nm, because the quasi-three-level transition induces strong thermal effects. Recently, we demonstrated that single-crystal fiber technology could significantly improve the available laser output at 946 nm in Nd:YAG, owing to an optimized thermal management allowed by the crystal geometry and packaging [5,6]. In this Letter, we propose to use a Nd:YAG single-crystal fiber Q-switched oscillator at 946 nm as a source for efficient fourth-harmonic generation. We show that this leads to an order of magnitude increase over previously reported results both in pulse energy and average power at 236.5 nm.

The experimental setup is displayed in Fig. 1. The laser is a Q-switched oscillator at 946 nm based on a Nd:YAG single-crystal fiber [6]. It emits an average power of 9.2 W in a linearly polarized beam at a repetition rate of 20 kHz, with a pulse width of 45 ns. The beam profile is Gaussian with a measured beam quality of $M^2x = 1.11$ and $M^2y = 1.13$ (Fig. 3). The pulse energy is 460 µJ, corresponding to a peak power of 10.2 kW.

Several crystals are commercially available to perform second-harmonic generation (SHG) to the visible range. We consider three crystals: lithium tetraborate LiB_3O_5 (LBO), bismuth borate BiB_3O_5 (BiBO), and periodically poled titanium phosphate (PPKTP). Their material and nonlinear properties are displayed in Table 1.

LBO is the most commonly used nonlinear crystal for visible SHG. While its nonlinearity is low compared to the other two crystals ($d_{eff} = 0.81$ pm/V), it has low walk-off, large angular acceptance, a very high damage threshold, and can be manufactured in large dimensions with very good optical quality. In contrast, BiBO has a large nonlinear coefficient ($d_{eff} = 3.34$ pm/V), but suffers from a large walk-off and low angular acceptance, often resulting in elliptical output beam. This also lowers the conversion efficiency for tight focusing when compared to crystals with a lower walk-off value. Furthermore, BiBO is a hygroscopic crystal that cannot be exposed to ambient air for a very long period of time.
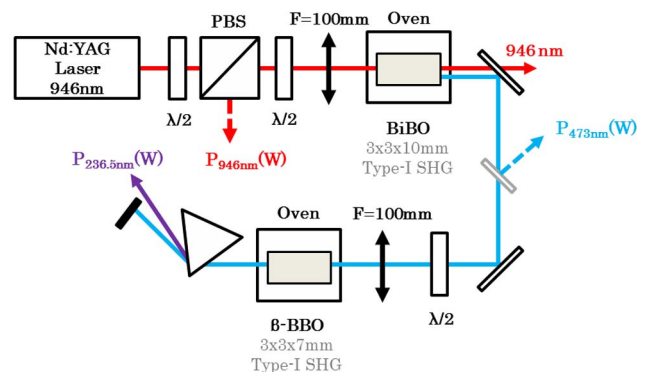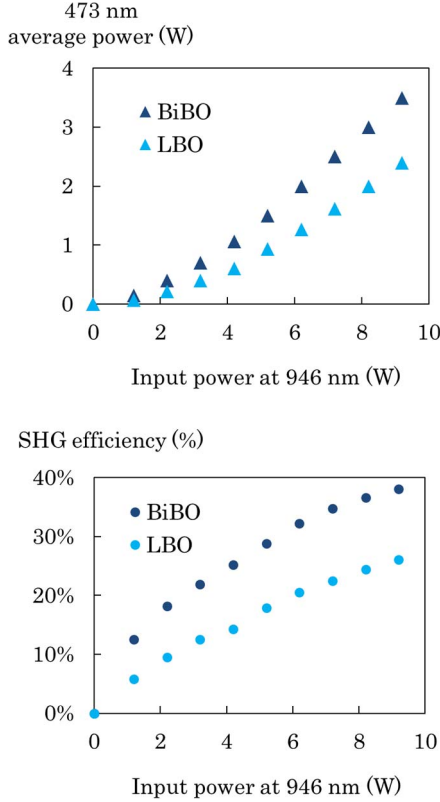

Fig. 1. Experimental setup.

Fig. 2. Average power (triangles) and conversion efficiency (circles) from 946 to 473 nm with BiBO.

Photorefractive damages have also been reported in BiBO [7]. Finally, periodically poled crystals such as PPKTP [8] benefit from a very large nonlinear coefficient ($d_{\mathrm{eff}} = 10$ pm/V), large angular acceptance as well as no walk-off, but have a low damage threshold, exhibit absorption in the visible range [9], and suffer from severe photorefractive damage (gray-tracking) at high power. Two crystals that have been used for conversion in the blue region have not been considered, namely KBO [10] and BBO [11], because they show inferior properties when compared to the other three crystals.
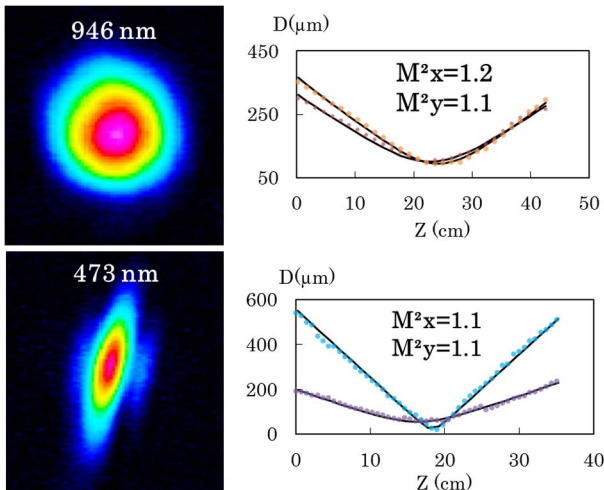

Fig. 3. Beam profiles and beam qualities at 946 and 473 nm after SHG in the 10 mm BiBO crystal.

Table 1. Material and Nonlinear Properties of Crystals for Blue SHG (QPM = Quasi-Phase-Matched)

Crystal	LBO	BiBO	PPKTP
Phase-matching type	Birefringent	Birefringent	QPM
Hygroscopy	Slight	Moderate	None
Photorefractive sensitivity	Very low	Reported	Severe
Visible absorption	Low	Low	High
d_{eff} (pm/V)	0.81	3.34	10
Walk-off (mrad)	11.3	40	0

The choice of a nonlinear crystal is strongly dependent on the fundamental laser source. For example, PPKTP is very useful at low powers, while LBO is more reliable in long-term operation at very high powers and is not subject to photorefractive damage. We choose to eliminate PPKTP from our choice list, because our peak power value is enough to use birefringent crystals in efficient configurations.

LBO and BiBO have therefore been experimentally compared. The LBO is a 3 mm × 3 mm × 20 mm crystal cut at $\theta = 90°$, $\varphi = 19.3°$ for type I SHG, with antireflective (AR) coatings at 946 and 473 nm. The BiBO is a 3 mm × 3 mm × 10 mm crystal cut at $\theta = 161.6°$, $\varphi = 90°$ for type I SHG, with AR coatings at 946 and 473 nm.

The 946 nm laser output is collimated, and a half-wave plate (HWP) in combination with a polarizer is used to adjust the fundamental power. Another HWP is used to control the polarization state. The beam is focused into a nonlinear crystal placed in a temperature-controlled oven. Residual infrared radiation at the output of the nonlinear crystal is filtered with a dichroic mirror.

For each crystal, the focal spot size must be chosen to maximize conversion efficiency. For a nonlinear crystal with length L, and a focused beam with Rayleigh range Zr, Boyd and Kleinman defined the optimal focusing condition as [12]

$$\xi = \frac{L}{2Zr} = 2.84.$$

In our case, for 20 mm LBO and 10 mm BiBO, this translates into focused beam diameters of 70 and 50 μm, respectively. Unfortunately, these values cannot be used because the corresponding input fluence would result in optical damage of the AR coatings. We therefore choose the minimum possible beam diameter, with an energy density limit of 5 J/cm^2 on the crystals input facet. The beam is focused down to a beam diameter $2\omega 0 = 125$ μm (defined at $1/e^2$). The BiBO crystal allows the most efficient SHG, with a conversion efficiency of 38% resulting in a maximum output power of 3.5 W (175 μJ) at 473 nm. The LBO crystal maximum output power at 473 nm is 2.4 W with a conversion efficiency of 26%. This is expected given that LBO has a much lower d_{eff} than BiBO. Conversion efficiencies and resulting output powers for SHG in BiBO and LBO are displayed in Fig. 2.

In all cases, no damage is observed on the nonlinear crystals, and specifically no photorefractive damage is observed in the BiBO crystal. Therefore, we choose the BiBO crystal for the SHG stage since it results in a

higher blue laser output power. We now focus on beam profile characterization at the output of the BiBO SHG stage.

As expected from the narrow acceptance angle of BiBO, the output 473 nm beam profile is elliptical. The beam quality at 4σ, measured with an automatic Dataray M^2 bench, is $M^2x = 1.14$ and $M^2y = 1.11$ (see Fig. 3). The pulse duration is shortened to 34 ns.

The blue beam is then filtered from the infrared with two dichroic mirrors. A wedged window is inserted in the beam path to measure the power at 473 nm incident on the second SHG stage (Fig. 1). The choice of a nonlinear crystal for frequency doubling from 473 to 236 nm is fairly straightforward, since beta barium borate (BBO) crystals and cesium lithium borate (CLBO) are the only commercial crystals with phase-matched configurations for that process. An experiment of fourth-harmonic generation from 946 to 236 nm was reported using CLBO crystals [13], but it requires cooling at –15°C, which increases the setup complexity and reduces the CLBO lifetime. Indeed, CLBO crystals are very hygroscopic and must be maintained at high temperatures [14].

BBO has a significant nonlinear coefficient ($d_{\mathrm{eff}} = 1.5$ pm/V) for frequency conversion from 473 to 236.5 nm. This should ensure large conversion efficiency even at a moderate blue peak power of 5 kW in a single-pass configuration. We therefore use a 7 mm long BBO, cut for type-I SHG from 473 to 236.5 nm at $\theta = 57.5°$. The crystal is placed in a temperature-controlled oven at 100°C to limit the nonlinear absorption effects occurring at high intensities and repetition rate [15]. It is AR-coated at 473 and 236 nm.

The elliptical output beam from the BiBO crystal is focused into the BBO crystal with a lens of focal length $f = 100$ mm, resulting in a beam size of 200 μm in the walk-off plane and 90 μm in the other transverse plane. An AR-coated HWP is used to adjust the input polarization. The output blue and ultraviolet beams are separated using a CaF_2 prism.

The output UV power and conversion efficiency are shown as a function of input power in Fig. 4. When the beam is focused tightly perpendicular to the walk-off plane, the output average power is 600 mW at 236.5 nm and a repetition rate of 20 kHz, corresponding to an energy of 30 μJ, and a fourth-harmonic total conversion efficiency of 6.5%. The corresponding conversion efficiency from 473 to 236.5 nm is 20%, which is the best
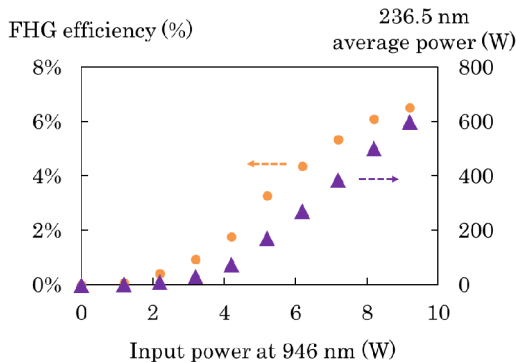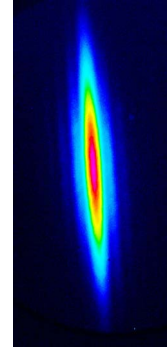

Fig. 5. Beam profile at 236.5 nm.

conversion efficiency reported so far for this process [3,4,13]. We observe a slight roll-off in the conversion efficiency at high power, which is expected from the combination of tight focusing and high walk-off value.

Since BBO crystals suffer from low acceptance angle (0.35 mrad.cm) and large walk-off (80.6 mrad for the UV beam), the orientation of the focused elliptical beam with respect to the walk-off plane must be carefully adjusted. Indeed, if the input elliptical beam is focused tightly in the walk-off plane, the output UV power is lowered to 440 mW.

The final UV pulse width is 27 ns and we observed an expected decrease of pulse widths by a factor close to 0.7 for each conversion stage. The beam profile in the UV was measured with a UV beam converter from Dataray and is displayed in Fig. 5. It is elliptical as expected.

The output power stability at 236.5 nm was measured for 2 h (see Fig. 6) and no signs of UV-induced degradation or pump laser power drop were observed. Power fluctuations seem to increase at the end of the stability measurement and we attribute this to the beginning of UV-induced BBO surface contamination.

More sophisticated crystal packaging, such as sealed environment, controlled atmosphere, and protection layers on the crystal facets, should improve the crystal lifetime. The optimum phase-matching temperature does not change as a function of input power, indicating that thermal effects do not induce a thermal gradient larger than the crystal thermal acceptance [16].

In conclusion, we report on a 236 nm pulsed laser based on a Nd:YAG single-crystal fiber Q-switched

Fig. 4. Average power (triangles) and conversion efficiency (circles) from 946 to 236.5 nm for BBO.
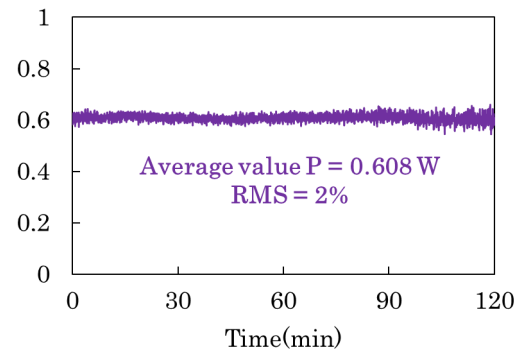

Fig. 6. Stability of the UV average power.

oscillator at 946 nm followed by a fourth-harmonic generation experiment using a BiBO and BBO combination. We obtain a stable 600 mW, 30 µJ deep-UV laser, at a repetition rate of 20 kHz, with a pulse width of 27 ns. This represents an improvement of more than 1 order of magnitude in average power and energy (30 times and 60 times, respectively) when compared to previously reported results [3]. It should be noted that previous state-of-the-art results were obtained in a much more compact, passively Q-switched experimental setup. Our laser source is suitable for spectroscopic measurements of dangerous compounds. Further possible improvements include an 885 nm pumping scheme for the 946 nm oscillator [17] and optimizing the last conversion stage with walk-off-compensated BBO [18].

References

1. C. M. Wynn, S. Palmacci, R. R. Kunz, K. Clow, and M. Rothschild, Appl. Opt. **47**, 5767 (2008).
2. C. M. Wynn, S. Palmacci, R. R. Kunz, and M. Rothschild, Opt. Express **18**, 5399 (2010).
3. S. Johansson, S. Bjurshagen, C. Canalias, V. Pasiskevicius, F. Laurell, and R. Koch, Opt. Express **15**, 449 (2007).
4. O. Kimmelma, I. Tittonen, and S. C. Buchter, J. Eur. Opt. Soc. Rapid Pub. **3**, 08008 (2008).
5. X. Délen, I. Martial, J. Didierjean, N. Aubry, D. Sangla, F. Balembois, and P. Georges, Appl. Phys. B **104**, 1 (2011).
6. L. Deyra, I. Martial, J. Didierjean, F. Balembois, and P. Georges, Opt. Lett. **38**, 3013 (2013).
7. J. H. Jang, I. H. Yoon, and C. S. Yoon, Opt. Mater. **31**, 781 (2009).
8. R. Le Targat, J.-J. Zondy, and P. Lemonde, Opt. Commun. **247**, 471 (2005).
9. G. Hansson, H. Karlsson, S. Wang, and F. Laurell, Appl. Opt. **39**, 5058 (2000).
10. G. Hollemann, E. Peik, and H. Walther, Opt. Lett. **19**, 192 (1994).
11. X. Ding, R. Wang, H. Zhang, W. Q. Wen, L. Huang, P. Wang, J. Q. Yao, X. Y. Yu, and Z. Li, Opt. Express **16**, 4582 (2008).
12. G. D. Boyd and A. D. Kleinman, J. Appl. Phys. **39**, 3597 (1968).
13. D. C. Gerstenberger, T. M. Trautmann, and M. S. Bowers, Opt. Lett. **28**, 1242 (2003).
14. Y. Morimoto, S. Miyazawa, and Y. Kagebayashi, J. Mater. Res. **16**, 2082 (2001).
15. M. Takahashi, A. Osada, A. Dergachev, P. F. Moulton, M. Cadatal-Raduban, T. Shimizu, and N. Sarukura, Jpn. J. Appl. Phys. **49**, 080211 (2010).
16. L. Deyra, I. Martial, F. Balembois, J. Diderjean, and P. Georges, Appl. Phys. B **111**, 573 (2013).
17. V. Lupei, G. Aka, and D. Vivien, Opt. Commun. **204**, 399 (2002).
18. S. Dutta Roy and S. Gangopadhyay, Appl. Phys. B **97**, 129 (2009).